Universiteit
Leiden
The Netherlands

Unravelling the collagen network of the arterial wall

Beenakker, J.W.M.

Citation

Beenakker, J. W. M. (2012, June 5). *Unravelling the collagen network of the arterial wall*. *Casimir PhD Series*. Retrieved from https://hdl.handle.net/1887/19050

Version:	Not Applicable (or Unknown)
License:	Leiden University Non-exclusive license
Downloaded from:	https://hdl.handle.net/1887/19050

Note: To cite this publication please use the final published version (if applicable).

Cover Page

Universiteit Leiden

The handle http://hdl.handle.net/1887/19050 holds various files of this Leiden University dissertation.

Author: Beenakker, Jan Willem Maria
Title: Unravelling the collagen network of the arterial wall
Date: 2012-06-05

7 Collagen remodeling and tumor micrometastasis in a zebrafish xenograft model

Part of this chapter is currently in press as:
Neutrophil-mediated experimental metastasis is enhanced by VEGFR inhibition in a zebrafish xenograft model
S. He, G. E. M. Lamers, J. W. M. Beenakker, C. Cui, V. P. S. Ghotra, E. H. J. Danen, A. H. Meijer, H. P. Spaink and B. E. Snaar-Jagalska
Journal op Pathology, 2012

7.1 Abstract

To study the dynamic and reciprocal interactions between tumor cells and their microenvironment, we used a xenograft model by injecting tumor cells into the blood circulation of transparent zebrafish embryos. This reproducibly results in rapid simultaneous formation of a localized tumor and experimental micrometastasis, allowing time-resolved imaging of both processes at single-cell resolution within one week. The tumor vasculature was initiated de novo by remodeling of primitive endothelial cells into a functional network. Roles of myeloid cells in critical tumorigenesis steps such as vascularization and invasion were revealed by genetic and pharmaceutical approaches. We discovered that the physiological migration of neutrophils controlled tumor invasion by conditioning the collagen matrix and forming the metastatic niche, as detected by two-photon confocal microscopy and second harmonic generation.

7.2 Introduction

The dynamic and reciprocal interactions between malignant tumor cells and the non-malignant cells in their microenvironment have a central role in tumor progression.[1, 2] Tumor cells secrete pro-angiogenic factors including the vascular endothelial growth factor (VEGF) to activate the endothelial cells of neighboring blood vessels and trigger angiogenesis to form tumor neovasculatures.[3] The tumor stromal cells, including fibroblasts and bone-marrow derived cells (MBDC), can secrete pro-angiogenic factors and control the angiogenic switch.[4, 5] Bone marrow-derived endothelial progenitor cells also participate in tumor vascularization by de novo vasculogenesis and/or direct incorporation into the tumor vasculature.[6, 7] Moreover, the myeloid lineages of BMDC are recruited by tumor cells to enhance their survival and aggressiveness.[3] The CD11+GR1+ myeloid cells, including immature dendritic cells, monocytes, neutrophils and early myeloid progenitors, promote tumor progression independent of the adaptive immune system and are essential mediators of the tumor refractoriness to anti-VEGF treatment.[7]

However, as these cells usually locate in deep tissues and can be functionally interfered by invasive detection methods, in vivo kinetic study of their actual roles in tumor progression remain challenging. Therefore, non-invasive visualization of the kinetic interaction between tumor cells and their microenvironment at high resolution will largely improve our understanding of the basic cancer biology and help to design new therapeutic strategies.

The zebrafish, Danio rerio, has been an important animal model for can-

cer, immune and stem cell research over the last decade.[8–11] Many molecular and cellular components that operate during tumorigenesis are conserved between zebrafish and mammals. A wide range of pharmacologically active compounds elicit physiological responses in zebrafish embryos comparable to those in mammalian systems,[12] making zebrafish ideal for identifying clinically relevant genes and compounds that regulate tumor progression. The transparency of zebrafish, in combination with the availability of various tissue-specific fluorescent reporter transgenic lines,[13, 14] allows high resolution in vivo analysis of tumor progression and the interactions between tumor cells and the host microenvironment.[15, 16] Several tumor transplantation assays with human and mammalian cells have been developed to study different aspects of tumor malignancies in embryo and adult zebrafish, such as tumor cell migration, proliferation, angiogenesis and tumor cell extravasation.[13, 15–19] However, most of these assays are limited to one selected step of tumor development and do not represent the full complexity of tumorigenesis in one model. In addition, for zebrafish embryonic engraftment models there are no reports published describing tumor cells extravasation from the circulation and invasion into the surrounding tissue where cells proliferate to form experimental metastases.

We have established a rapid, reproducible zebrafish embryonic xenograft model for simultaneous formation of a localized tumor and experimental micrometastasis by intravascular injection of tumor cells into the blood circulation of zebrafish embryos. With non-invasive high-resolution imaging we characterized the critical steps of tumor progression, including tumor vascularization and tissue invasion. Using this model, we found that myeloid cells are involved in these tumor processes, and especially that neutrophils condition the collagen matrix to facilitate metastatic niche formation and tumor invasion.

7.3 Results

Intravascular injection of tumor cells into zebrafish embryos resulted in localized tumor growth and micrometastasis within 6 days

In order to develop an experimental metastasis model, as frequently used in mice, we implanted up to 400 fluorescent tumor cells into the blood circulation of zebrafish embryos at 2 day post fertilization (dpf). The tumor cells hematogenously disseminated in the embryo immediately after injection into the duct of Cuvier, a wide circulation channel on the embryonic yolk sac connecting the heart to the trunk vasculature (fig. 7.1A,B). When > 100 tumor cells were injected, the embryonic circulation was not sufficient to disseminate the entire bulk of implanted cells, resulting in the accumulation of non-disseminated cells close

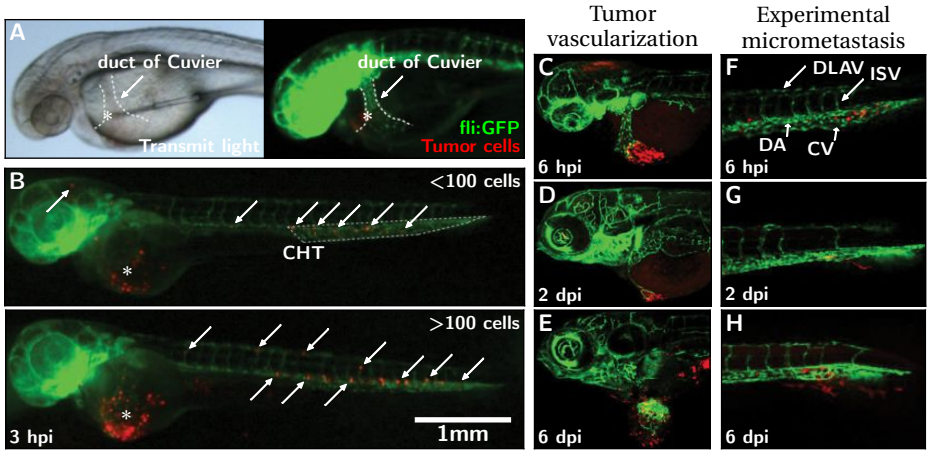

Figure 7.1:
(A) Bright field (left) and fluorescence (right) images showing the injection of tumor cells (red) into the zebrafish embryonic circulation (green) via the ventral side of the duct of Cuvier.
(B) Dissemination of implanted tumor cells in embryos injected with ≤ 100 (top) or > 100 cells. Dissemination was observed in almost all embryos (124/125) at 3 hours post implantation (hpi). The injection sites are indicated by * and disseminated tumor cells are indicated by arrows. The caudal hematopoietic tissue (CHT) is outlined (top). Note that tumors also accumulated close to the injection site in the example of an embryo injected with > 100 cells (bottom).
(C–E) Progression of tumor formation. Tumor cells accumulated close to the injection site at 6 hpi (C), induced formation of neovasculature at 2 days post implantation (dpi) (D), and displayed localized tumor growth at 6 dpi (E).
(F–H) Formation of micrometastases. Disseminated tumor cells resided in the tail at 6 hpi (F), invaded into the neighboring tail fin at 2 dpi (G), and formed micrometastasis colonies in the fin tissue at 6 dpi (H).
Red in A,B&E: tumor cells labeled with the red cell tracker CM-DiL.; Red in C,D,F–H: tumor cells stably expressing dsRed. Green in all: GFP-endothelial cells of the Tg(Fli:GFP) line. Abbreviations: DLAV: dorsal longitudinal anastomotic vessel; ISV: intersegmental vessel; DA: dorsal aorta; CV: caudal vein.

to the injection site at the duct of Cuvier (fig. 7.1B). Using a Tg(Fli:GFP) endothelial reporter transgenic zebrafish line with fluorescent vasculature,[13] we found that the accumulated tumor cells induced neovasculature formation and developed into a localized tumor (fig. 7.1C-E), whereas the disseminated tumor cells formed micrometastic colonies in the trunk of the fish (fig. 7.1F-H). Localized tumor growth and experimental micrometastases were also induced by several other types of mouse- or human-originated tumorigenic cell lines, but never by non-malignant cell lines (table 7.1). This novel experimental metastasis assay bypasses the primary tumor stage and intravasation, but opens the possibility to use this model to screen for anti metastatic agents in a few days instead of weeks in rodent models.

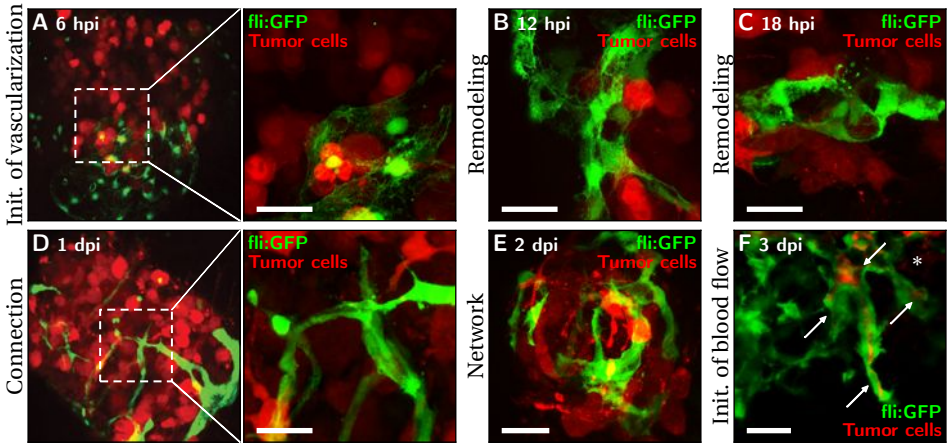

Figure 7.2:
(A–E) Initiation of tumor-induced neovasculature. Fli:GFP embryos were imaged from the ventral side to achieve a top view of dsRed labeled FGF-T-MAE tumor cells, which, after implantation, accumulated under the primitive endothelial cells of the duct of Cuvier (A, 6 hpi, with magnification in the right panel). At 12 hpi, the primitive endothelial cells in close association with the tumor cells started to change morphology (B). At 18 hpi, the primitive endothelial cells were remodeled into vessel-like structures (C; 3 connected GFP-endothelial cells). The remodeled endothelial cells were further connected within the tumor cell mass at 1 dpi (D, with magnification in the right panel). At 2 dpi, a partially lumenized vasculature network had formed within the tumor cell mass (E).
(F) Microangiography with tetramethylrhodamine dextran showing partial blood flow in the tumor vessels at 3 dpi (red, indicated by arrows). Some leakage of the tumor vessels was also observed (*).
Scale bars: 25 µm.

Cell line	Description	Vascularization/localized tumor growth	Tumor invasion/micrometastasis	*n*
KFGF-T-MAE	MAE cells transformed by FGF2 over expression	97.0%	32.8%	67
4T1	Mouse breast cancer	64.7%	15.5%	142
MDA-MB-231	Human breast cancer	0%	47.9%	48
PC3	Human prostate cancer	25.0%	0%	60
MAE	Mouse endothelial	0%	0%	>100
ZF4/PAC2	Zebrafish fibroblast cell lines	0%	0%	>100

Table 7.1:
The migratory potential of various tumor cells. For every tumor cell type the cells have been implanted in *n* different fish at 2 days post fertilization (dpf). 6 day post implantation the fish were scored for vascularization/localized tumor growth and tumor invasion/micrometastasis. (data not shown[20])

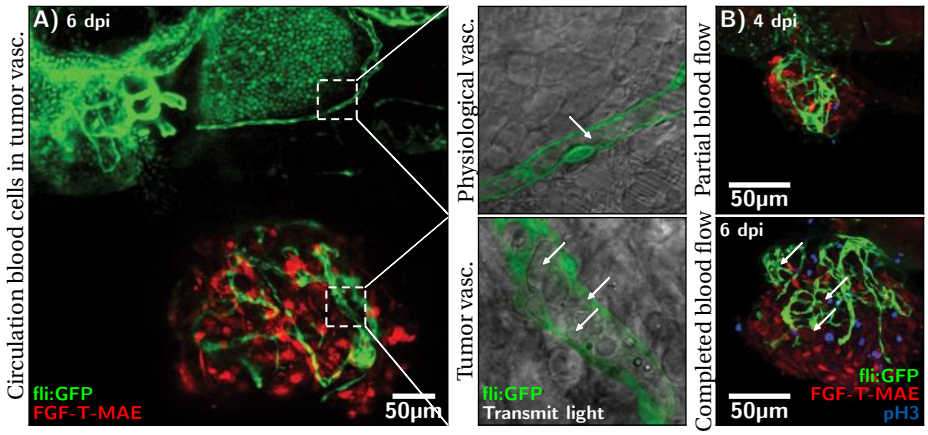

Figure 7.3:
(A) An expanded tumor mass of FGF-T-MAE-mCherry cells, supported by a functional vasculature-network, at 6 dpi. The right panel shows magnifications of a pectoral fin vessel (top) and a tumor vessel (bottom). Circulating blood cells within the vessels are indicated by arrows (overlay of transmitted light and GFP channel).
(B) Phosphohistone H3 (pH3, blue) staining of Fli:GFP embryos implanted with FGF-T-MAE-mCherry cells. The pH3+ staining, as a marker of proliferation, was increased in both mCherry+ and mCherry- cell populations after 4 dpi, when circulating blood cells started to be detected in the tumor neovasculature.

Tumor vascularization is the critical step for localized tumor growth

Taking advantage of the transparency of zebrafish embryos, we performed high-resolution confocal imaging to characterize the localized tumor growth. Shortly after implantation, the non-disseminated tumor cells locally accumulated in close association with the primitive endothelial cells of the duct of Cuvier (fig. 7.2A), which were subsequently remodeled into neo-vessel-like structures by the tumor cells (fig. 7.2B,C). Subsequently the neo-vessels connected and gradually formed an irregular, tortuous, lumenized vasculature network within 2 days (fig. 7.2D,E). Partial blood flow was detected in the tumor vasculature by microangiography from 3 days post implantation (dpi) (fig. 7.2F) and circulating erythrocytes were observed in the lumen after 4 dpi (fig. 7.3A).

Notably, only in the embryos where such functional tumor neovasculature had formed, the localized tumor cells expanded into a tumor mass of > 0.15 mm diameter by 6 dpi. Phosphorylation of histone H3 (pH3), a proliferation marker, significantly increased in both fluorescence-positive tumor cells and fluorescence-negative stromal cells of the localized tumor mass after 4 dpi (fig. 7.3B), when the tumor vasculature started to be functional. These results indicate that suc-

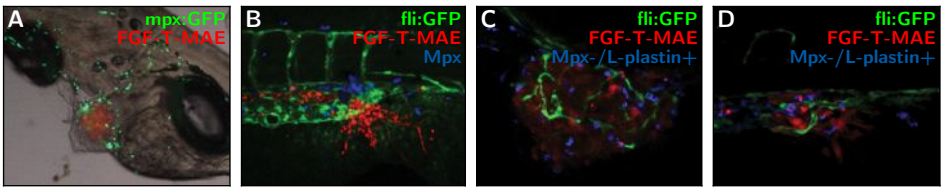

Figure 7.4:
(A) Neutrophils (green, Tg(mpx:GFP)^{i114}) associated with FGF-T-MAE tumor cells (red) at the localized tumor growth site.
(B) Neutrophils (blue, Mpx+ histochemical staining) associated with the tumor cells (red) at the micrometastasis site.
(C–D) Macrophages (blue, Mpx-/L-lpastin+) associated with the tumor cells (red) at the localized tumor (C) and the micrometastasis (D) sites.

cessful tumor vascularization was the critical step for localized tumor growth in our model. Importantly, this de novo, tumor induced vascularization represents a totally different phenomenon than a previously described angiogenesis assay, which monitors growth of new vessels from existing vessels towards tumor implant.[21]

Myeloid cells are involved in tumor vascularization and invasion

Leukocytes are known to contribute to different steps of tumor progression including the formation of tumor vasculature and metastasis.[2, 4, 5, 7] In zebrafish embryos, the caudal hematopoietic tissue (CHT) is known as a transient site of hematopoiesis and leukocyte differentiation.[17] Our observation that tumor cell invasion occurred at the posterior end of the CHT suggested involvement of leukocytes in tumor progression. In the first few days of zebrafish development, macrophages and neutrophils are the only populations of functional leukocytes in the embryos.[18] Using a combination of myeloid lineage markers (Mpx+ for neutrophils and Mpx-/L-plastin+ for macrophages[19]) we detected that FGF-T-MAE tumor cells were accompanied by cells of the myeloid lineages both at the localized tumor growth site near the site of implantation, and at the invasion site at the posterior end of the CHT (fig. 7.4).

To investigate the role of myeloid cells in tumor progression, we used morpholino oligonucleotides to knockdown the transcription factor Pu.1, which controls the development and differentiation of myeloid cells in zebrafish embryos.[22] As previously shown, Pu.1 knockdown is most effective in suppressing macrophage differentiation; while neutrophil differentiation can be suppressed only under maximal knockdown conditions.[23] In agreement, in our experiments macrophages were depleted in zebrafish embryos up to 3 dpf by a partial knock-

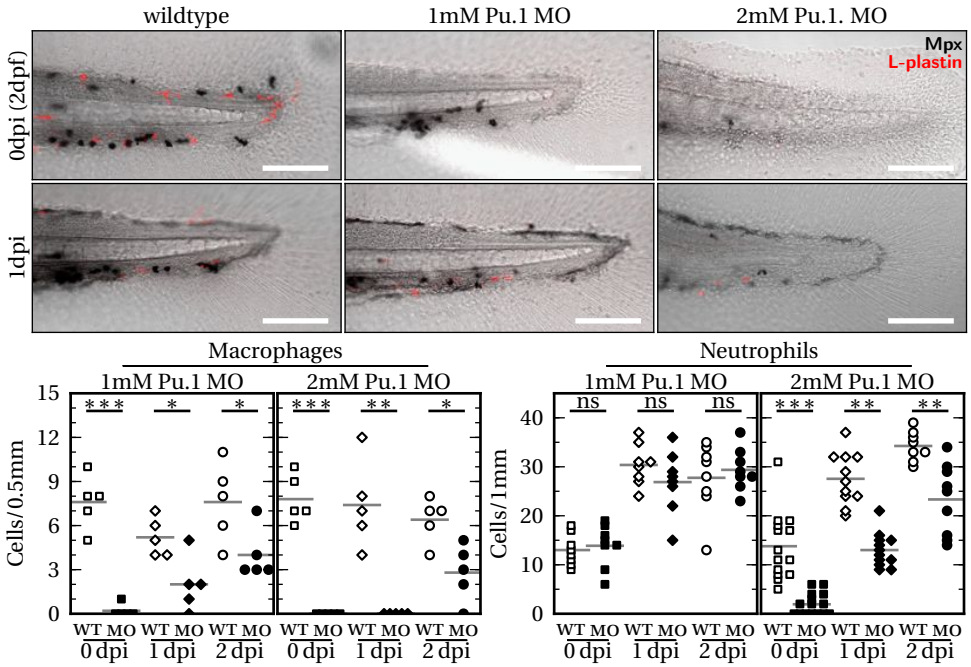

Figure 7.5:
Lineage-specific depletion of macrophages and neutrophils by dose-dependent morpholino-mediated knockdown of Pu.1. Neutrophils are shown in black (Mpx+ histochemical staining) and macrophages are shown in red (Mpx-/L-lpastin+). In each embryo, the macrophages in the region 0.5 mm from the posterior end of the tail fin and the neutrophils in the region 1 mm from the posterior end of the tail fin were quantified, which are sufficient to represent each linage distribution in the entire embryo.
Scale bars: 100 µm; ns = not significant ($p > 0.05$); * = $0.01 < p < 0.05$; ** = $0.0001 < p < 0.01$; *** = $p < 0.0001$.

down of Pu.1 (1 mM morpholino; fig. 7.5), while neutrophils were depleted by the complete knockdown of Pu.1 (2 mM morpholino; fig. 7.5). Using these different doses of Pu.1 morpholino, we found that the formation of tumor neovasculature, but not the physiological vasculature, was impaired under both partial and complete knockdown conditions of Pu.1 (fig. 7.6A, B), suggesting a major role of macrophages in the tumor vascularization. In contrast, tumor cell invasion at the posterior end of the CHT was only suppressed by complete knockdown of Pu.1, not by partial knockdown (fig. 7.6C,D), indicating that neutrophils play a predominant role in tumor cell invasion and micrometastasis. Taken together, myeloid cells are involved in the processes of both tumor vascularization and invasion, the critical steps towards localized tumor growth and micrometastasis.

A previous study of zebrafish myeloid cells sensing of HRASG12V-transformed

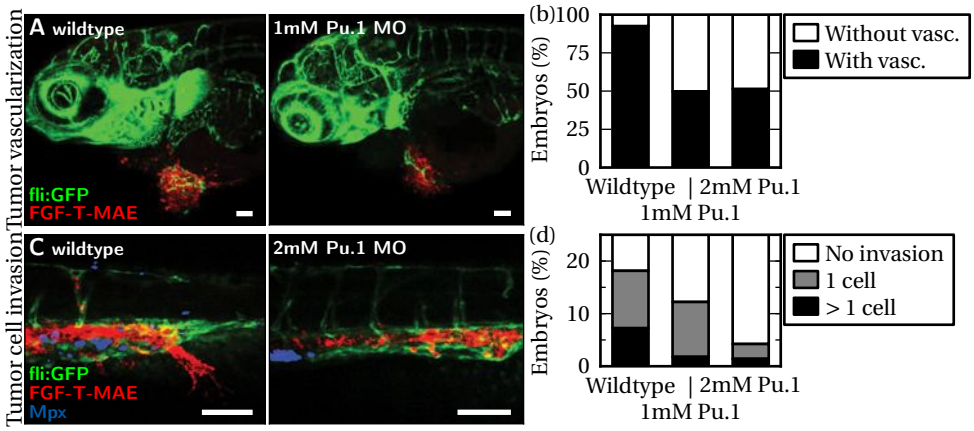

Figure 7.6:
(A,B) Suppression of FGF-T-MAE tumor vascularization under partial (1 mM) or complete (2 mM) knockdown of Pu.1 was significant (Wilcoxon test, $p < 0.01$). Representative embryos with tumor vascularization in the control and Pu.1 knockdown conditions at 3 dpi are shown in A and quantification of embryos with and without tumor vascularization at 1 dpi are shown in B.
(C,D) Suppression of FGF-T-MAE tumor cell invasion at the posterior end of the CHT under complete knockdown of Pu.1 was significant (Wilcoxon test, $p < 0.01$). Representative control and Pu.1 knockdown embryos at 1 dpi (C) and embryos scored for tumor cell invasion at 1 dpi (D). Scale bars are approximately 100 µm.

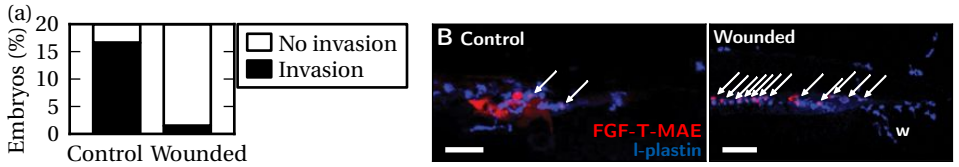

Figure 7.7:
(A) Suppression of tumor cell invasion by wound-inflammation in the tail fin at 1 dpi was significant (Wilcoxon test, $p < 0.001$). A wound in the tail fin was made mechanically (as in fig. 7.11) just after implantation of tumor cells at 2 dpf.
(B) Phagocytosis of tumor cells (indicated by arrows) around the invasion site by myeloid cells in embryos in which the tail fin was wounded (positioned by W). Tumor cells are shown in red and myeloid cells were stained for L-plastin (blue). Scale bars are approximately 200 µm.

cells suggested homologies between the myeloid cell responses towards transformed cells and wound-induced inflammation.[15] Therefore, we investigated the influence of wound-induced inflammation on tumor progression in our model. When the embryos were wounded at the tail-fin, we observed that tumor cell invasion was largely suppressed or abolished (fig. 7.7A). This suppression of tumor invasion was probably caused by inflammation-enhanced myeloid cell

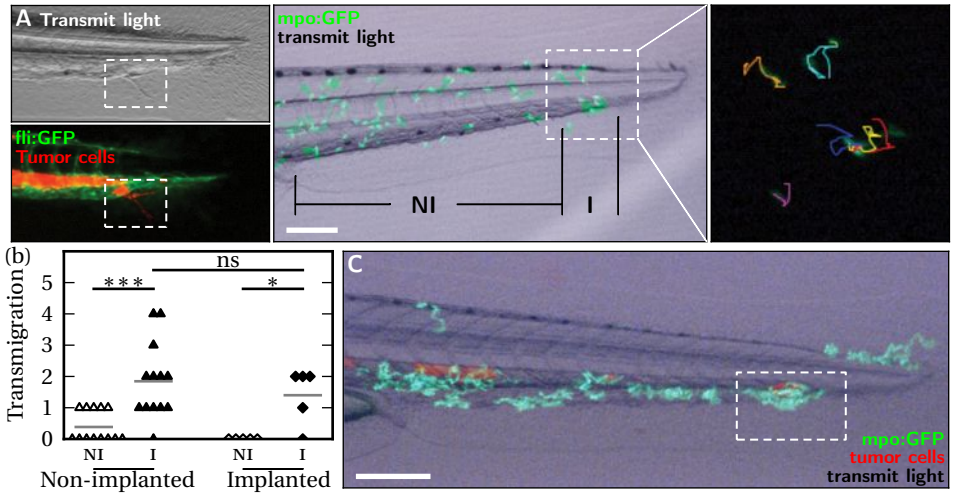

Figure 7.8:

(A) Migration tracks of GFP+ neutrophils in the tail of a Tg(mpx:GFP)^{i114} embryo (30 min time lapse with 1 min intervals). GFP+ neutrophils only transmigrated between the caudal hematopoietic tissue (CHT) and the tail fin (TF) at the site where tumor cells invaded into the tail fin. The CHT-TF transmigration area is indicated in the left panel which shows invasion of the tail fin by a dsRed-labeled FGF-T-MAE cell in a 3 dpf Tg(fli:GFP) embryo (top: bright field; bottom: fluorescence image). Manual tracking of 30 min migration patterns (right panel) of GFP+ neutrophils in the highlighted region of the tail of a 3 dpf Tg(mpx:GFP)^{i114} embryo (middle panel) showed that the transmigrating neutrophils (red, yellow and blue tracks) migrated as randomly as neighboring neutrophils in the tail (orange and light blue tracks) or already inside the fin tissue (purple track).

(B) Quantification of neutrophil transmigration (in 30 min) into the tail fin. Time lapse recordings were made of 3 dpf Tg(mpx:GFP)^{i114} embryos with or without implanted FGF-T-MAE tumor cells and the number of times that GFP+ neutrophils crossed the CHT-TF boundary was counted in two areas of the tail, the tumor invasion site (I) and the non-invasion site (NI) as indicated in A. The CHT-TF transmigration of neutrophils selectively occurred at the same site as tumor invasion. This spatial preference was not influenced by implantation.

(C) Two-hour recording of neutrophil (green) migration in Tg(mpx:GFP)^{i114} embryos after implantation of FGF-T-MAE tumor cells (red). The selective neutrophil CHT-TF transmigration site, overlapping with the tumor invasion site, is outlined.

ns = not significant ($p > 0.05$); * = $0.01 < p < 0.05$; ** = $0.0001 < p < 0.01$; *** = $p < 0.0001$.
Scale bars are approximately 200 µm.

phagocytosis, as the majority of implanted tumor cells were phagocytosed by L-plastin+ myeloid cells (fig. 7.7B). This result suggests that, in the absence of wounding, myeloid cells contribute to tumor vascularization and invasion in an inflammation-independent physiological manner.

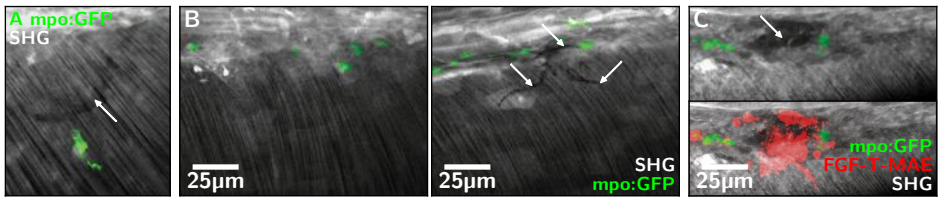

Figure 7.9:
Second harmonic generation (SHG) analysis of the fibrillar collagen matrix around the CHT-TF transmigration site. Images show an overlay of SHG signal (gray) with fluorescence of GFP+ neutrophils (TG(mpx:GFP)^{i114}) and red CM-DiL:-labelled FGF-T-MAE tumor cells.
(A) Example of a track (indicated by the arrow) of deformed collagen matrix in the tail fin created by a migrating neutrophil.
(B) Comparison of a region in the tail fin with no recent neutrophil migration events (left) and a region showing SHG-negative tracks (indicated with arrows) generated by migrating neutrophils (right).
(C) Invasion of tumor cells in an SHG-negative site in the tail fin. The image on the top shows the overlap of SHG and green fluorescence signal of neutrophils and the image on the bottom additionally shows the red fluorescence signal of tumor cells. The local loss of SHG signal is indicated with the arrow in the top image.

Physiological neutrophil migration conditions the collagen matrix for tumor cell invasion

To further investigate the involvement of neutrophils in tumor cell invasion, the physiological migration of neutrophils in 3 dpf embryos was analyzed using the TG(mpx:GFP)^{i114} neutrophil-specific zebrafish reporter line.[14] Time lapse and trajectories analysis showed that neutrophils randomly transmigrated between the caudal hematopoietic tissue and the tail fin (termed as "CHT-TF transmigration"), as a part of their physiological unrestricted random migration. This non-directional motion of neutrophils selectively occurred at the posterior end of the CHT where the perivascular tumor cells invaded into the tail fin (fig. 7.8A, B). The spatial preference for this location of CHT-TF transmigration was not altered by tumor cell implantation (fig. 7.8B,C) or by wound-induced inflammation (unpublished data and [24, 25]), suggesting that it is the normal physiological property of neutrophil migration in zebrafish embryos.

To further decipher the impact of neutrophil CHT-TF transmigration on the spatially co-localized tumor cell invasion process, two-photon excited confocal microscopy and second harmonic generation (SHG) was performed to visualize the extracellular fibrillar collagen matrix upon neutrophil migration.[26] Migrating neutrophils created transient tracks of deformed collagen matrix, as detected by the loss of SHG signal (fig. 7.9A), which was previously reported to be sufficient to support tumor cell invasion in mice models.[27] As a consequence of

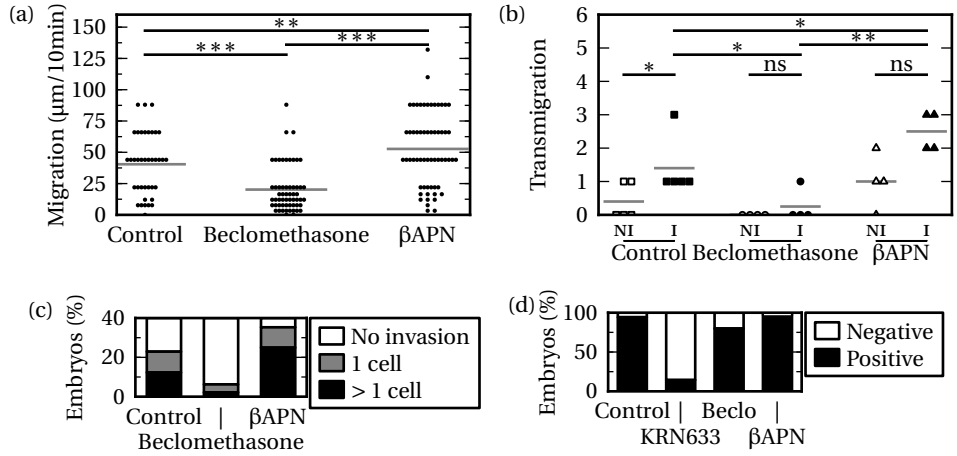

Figure 7.10:

(A) The random non-pathological migration of neutrophils was suppressed by beclomethasone (25µM) and promoted by βAPN (500µM). Migration tracks (µm) of neutrophils in 3dpf Tg(mpx:GFP)^{i114} embryos were recorded over 10min intervals.

(B) The CHT-TF transmigration of neutrophils (in 30min) was suppressed by beclomethasone and promoted by βAPN. Transmigration events in non-invasion (NI) and invasion (I) areas of the tail fin were quantified as in fig. 7.8B

(C) Tumor cell invasion at the posterior end of the CHT was significantly suppressed by beclomethasone (Wilcoxon test, $p < 0.01$) and promoted by βAPN($p < 0.01$). Embryos were scored for tumor cell invasion at 1dpi.

(D) Tumor vascularization was significantly suppressed by 0.1µM KRN633 (Wilcoxon test, $p < 0.01$), but not by 25µM beclomethasone or 500µM βAPN. Embryos were scored for vasculogenesis at 1dpi, as in fig. 7.6B.

ns = not significant ($p > 0.05$); * = $0.01 < p < 0.05$; ** = $0.0001 < p < 0.01$; *** = $p < 0.0001$.

the localized neutrophil CHT-TF transmigration, the deformation of the collagen matrix was largely enhanced at the posterior end of the CHT where the perivascular tumor cells invaded into the tail fin (fig. 7.9B). Furthermore, we observed that the tumor cells invaded into the tail fin at the exact site of local collagen deformation (fig. 7.9C). Thus, the observed tumor cell invasion was promoted by physiological neutrophil migration (the CHT-TF transmigration) which conditions the extracellular collagen matrix.

Pharmacological approaches were taken to confirm the functional involvement of neutrophil migration in tumor cell invasion. A prototype glucocorticoid receptor agonist beclomethasone, previously shown to inhibit neutrophil migration,[28] did not cause alteration of the fibrillar collagen matrix in zebrafish embryos (data not shown). We detected an inhibition of the normal physiological neutrophil migration and of neutrophil chemotaxis directed by wounding-induced inflammation[29] at 4 hours after administration of 25µM beclometha-

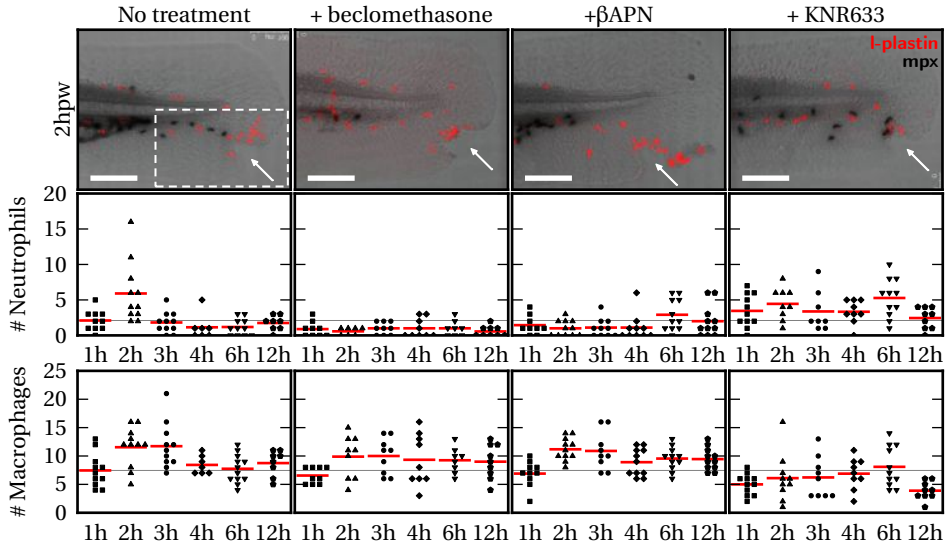

Figure 7.11:

Wounding-induced myeloid cell chemotaxis was affected by different pharmacological treatments. 3 dpf embryos were wounded on the tail fin as indicated by arrows in representative images of embryos from different treatment groups (no treatment; 25µM beclomethasone; 500µM βAPN; 1µM KRN633) at 2 hours post wounding (hpw). Embryos were fixed at different time point over a course of 12 hpw and stained for neutrophils (MPX+, histochemical staining) and macrophages (MPX-/L-lpastin+). Quantification of neutrophil and macrophage numbers was performed on $n \geq 8$ embryos per time point for each treatment group. The macrophages/neutrophils in the region outlined were quantified to measure the myeloid cell chemotaxis towards the wound.
Scale bars: 100µm

sone (fig. 7.10A,B and 7.11). Tumor cell invasion and micrometastasis was also reduced in embryos incubated in 25µM beclomethasone 4 hours before implantation (fig. 7.10C). In addition, we found that the lysyl oxidase inhibitor β-aminoproprionitrile (βAPN) largely reduced fibrillar collagen (unpublished data) and enhanced the CHT-TF transmigration of neutrophils, leading to a significant increase of tumor cell invasion and subsequent formation of micrometastases (figures 7.10A–C). Notably, βAPN inhibited neutrophil chemotaxis induced by inflammation (fig. 7.11), indicating that the increase of tumor cell invasion in βAPN-treated embryos was correlated with enhanced non-pathological neutrophil migration, but not with inflammation. Both beclomethasone and βAPN had no significant effect on macrophage chemotaxis (fig. 7.11) and tumor vascularization (fig. 7.10D). Taken together, these results reveal that only non-pathological neutrophil migration and the spatially restricted CHT-TF transmigration modify the extracellular matrix and have a major impact on tumor cell invasion and micrometastasis in this model.

7.4 Discussion

Using a novel zebrafish xenograft model that allows simultaneous single-cell resolution monitoring of multi-step tumorigenesis in vivo, including tumor vascularization, localized tumor growth, tumor invasion and micrometastasis formation, we discovered a new mechanism of the metastatic niche formation. In addition to the published roles of macrophages in this process,[2] we found that physiological migration of neutrophils controlled tumor invasion by conditioning the collagen matrix to facilitate the metastatic niche.

Recently the zebrafish myeloid cell population has been studied in detail and the similarities with the human myeloid cell functions and embryonic differentiation have been demonstrated.[30, 31] Further evidence that the zebrafish holds much potential for translational studies in cancer has been published.[32, 33] Recently it has been reported that expression of WHIM truncation mutations of CXCR4 in zebrafish neutrophils induces neutrophil retention in the caudal hematopoietic tissue, which represents a mechanism of human immunological WHIM disorder. WHIM zebrafish are neutropenic, and WHIM neutrophils show impaired recruitment to tissue inflammation sites, recapitulating the human disease. These findings support the potential of zebrafish to model primary immune disorders and underscore the translational relevance of zebrafish neutrophils transmigration in understanding of disease pathogenesis.[34, 35]

The involvement of myeloid cells in critical tumorigenesis steps such as vascularization and invasion was revealed by both genetic and pharmacological approaches. We demonstrated that myeloid cells, particularly the macrophages, are essential for tumor vascularization. Importantly, we also obtained evidence that the micrometastasis site was determined by the physiological migration of neutrophils. Our results show that yet undefined environmental cues favor neutrophil transmigration at the posterior end of the caudal hematopoietic tissue, which remodels the fibrillar collagen matrix, and in turn conditions the pre-metastatic niche for the tumor cells to invade into the tail fin. These findings support the “seed and soil” hypothesis that tumor metastasis is controlled by both the tumorigenic property of disseminated cells and their microenvironment.[36]

It is known that tumor-infiltrating immune cells can have both tumor-promoting and tumor-antagonizing roles.[37] In our model, the myeloid cells promote tumor progression under the physiological wound-free condition (fig. 7.6B,D), whereas immune-mediated destruction of tumor cells was hyper-activated by wound-induced inflammation (fig. 7.7). These results indicate that environmental factors have an impact on the balance between the conflicting immune cell responses to tumor cells. Interestingly, we found that the lysyl oxidase inhibitor

βAPN accelerates physiological neutrophil migration but decelerates pathological neutrophil chemotaxis, suggesting that different molecular mechanisms are involved in different modes of myeloid cell migration.

We propose that dual targeting of angiogenesis and myeloid cells can be beneficial in future treatments. Of course it will be only relevant for medical studies if the neutrophil transmigration is not restricted to this model. Currently the role of macrophages in intra- and extravasation of cancer cells is well established.[2] The role of neutrophils is less studied, however tumor associated neutrophils (TANS) were recently described and an increased level of neutrophils in cancer patients was shown to correlate with poor prognosis.[38] For example, a quantification of TANS in patients with renal cell carcinoma revealed that the presence of neutrophils correlated with increased mortality.[38] In addition, increased levels of TANS in the bronchioalveolar space of patients with bronchioalveolar carcinoma were significantly associated with poor outcomes.[39] In order to dissect the function of myeloid cells in human cancers live imaging of tumor-microenvironment interactions at the cellular level is required, a process severely limited in current mammalian models. This limitation strongly supports the relevance of the zebrafish model to unravel the molecular mechanisms of how tumor associated neutrophils mediate metastasis in zebrafish and mammalian models.

7.5 Materials and Methods

Zebrafish maintenance, morpholino injection and pharmacological treatment Zebrafish and embryos were raised, staged and maintained according to standard procedures in compliance with the local animal welfare regulations. The transgenic lines TG(FLI1:GFP) and TG(MPX:GFP)^{i114} were used in this study.[13, 14] 0.2mM N-phenylthiourea (PTU, Sigma) was applied to prevent pigment formation from 1 day post fertilization (dpf). For PU.1 knockdown as previously published, PU.1 MO (1MM for partial knockdown and 2MM for complete knockdown[22]) was injected into the yolk at the 1-cell stage as described.[40] For pharmacological inhibition, the VEGFR tyrosine kinase inhibitors KRN633 (0.1-1μM; Santa Cruz) or Sunitinib (0.1-1μM; Sigma), beclomethasone (25μM; Sigma), and β-aminopropionitrile (βAPN, 500μM; Sigma) were applied directly to the egg water and refreshed every two days.

Cell lines Murine aortic endothelial (MAE) cells and tumorigenic FGF2-overexpressing FGF2-T-MAE cells[21] (provided by M. Presta, University of Brescia, Italy), and the human breast carcinoma cell line MDA-MB-231[41] (provided by P. ten Dijke, Leiden University Medical Center, the Netherlands) were cultured as previously

described. 4T1 (CRL-2539, ATCC) and PC3 (CRL-1435, ATCC) cells were cultured in RPMI 1640 supplemented with 10% FBS (Invitrogen). Stable fluorescent cell lines were generated using lenti-viral vectors expressing dsRed or mCherry (provided by R. C. Hoeben, LUMC, the Netherlands). The virus-infected cells were used for experiments without FACS sorting and the fluorescence was stable in vitro for >10 passages. Zebrafish fibroblast cell lines ZF4 and PAC2 were cultured as previously described.[42]

Embryo preparation and tumor cell implantation Dechorionized 2 dpf zebrafish embryos were anesthetized with 0.003% tricaine (Sigma) and positioned on a 10 cm Petridish coated with 1% agarose. Mammalian cells were trypsinized into single cell suspensions, resuspended in PBS (Invitrogen), kept at room temperature before implantation and implanted within 3 hours. Non-fluorescent cells were labeled with the fluorescent cell tracker CM-DiL (Invitrogen) according to the manufacturer's instructions. The cell suspension was loaded into borosilicate glass capillary needles (1 mm O.D. × 0.78 mm I.D.; Harvard Apparatus) and the injections were performed using a Pneumatic Pico pump and a manipulator (WPI). 50~400 cells, manually counted, were injected at approximately 60 µm above the ventral end of the duct of Cuvier, where the duct of Cuvier opens into the heart. After implantation with mammalian cells, zebrafish embryos (including non-implanted controls) were maintained at 34 °C, to compromise between the optimal temperature requirements for fish and mammalian cells.[20] Up to 600 implantations were manually achieved per hour, with survival rates over 90% until 6 dpi. For pharmacological inhibition, beclomethasone was applied to the embryos 4 hours before implantation and KRN633, Sunitinib and βAPN were applied 4~6 hours post implantation. For each cell line or condition, data are representative of ≥3 independent experiments with ≥30 embryos per group. Experiments were discarded when the survival rate of the control group was less than 90%.

Microscopy and analysis For live imaging, embryos were anesthetized using 0.016% tricaine (Sigma) and mounted in 0.6% low melting agarose. Fixed embryos were imaged in PBST. Fluorescent image acquisition was performed using a Leica MZ16FA stereo microscope, a Leica TCS SPE confocal microscope or a Zeiss LSM exciter on an Axio Observer confocal microscope. Confocal stacks were processed for maximum intensity projections with Zeiss ZEN2009 software or ImageJ software. Images were adjusted for brightness and contrast using ImageJ. Overlays were created using Adobe Photoshop CS4 or ImageJ. 3D reconstruction and movies were assembled using ImageJ.

Multi-photon microscopy Second-harmonic generation (SHG) was used to image the helical structures of collagen fibers, which are capable of combining two photons into one.[26] The two-photon microscopy was performed on a Zeiss 710 NLO upright confocal microscope equipped with a Spectra-physics Deep See MP laser. The images were obtained with an excitation wavelength of 750 nm and only emitted light with a wavelength between 371 nm–467 nm was detected.

Myeloid cell detection In the Tg(fli1:GFP) line, the neutrophils in fixed embryos were detected using the Peroxidase/Myeloperoxidase Leukocyte Kit (Sigma) as described.[29] The embryos were imaged with transmitted light and the black stained cells were extracted using the Threshold function of ImageJ and subsequently converted into a selected color for overlay with fluorescence images. For macrophage detection, immunohistochemistry for L-plastin was performed after the myeloperoxidase activity assay and the MPX-/L-lpastin+ cells were counted as macrophages.[19] The Tg(mpx:GFP)^{i114} line was used to monitor neutrophil migration in vivo.[14] Time lapse imaging (1 minute intervals, ≥30 min) was performed using a Leica stereo fluorescence microscope. The migration tracks were generated by maximum intensity projections of the time stacks using ImageJ. For individual neutrophil tracking, the first 20 GFP+ cells from the posterior end of the tail fin in each embryo, which exhibited consistent intensity for at least 15 min, were tracked and analyzed using the Manual Tracking plugin of ImageJ.

Immunohistochemistry Whole-mount immunohistochemistry was carried out as described.[43] Primary antibodies and dilutions were used as follows: L-plastin (rabbit anti-zebrafish, 1:500; provided by A. Huttenlocher[19]), ZO-1 (mouse anti-human, 1:300; Invitrogen), phosphohistone H3 (rabbit anti-human, 1:500; Santa Cruz). 1:200 dilution of the secondary antibodies (Alexa 405 anti-mouse and Alexa 568 anti-mouse or Alexa 568 anti-rabbit; Invitrogen) was used for detection.

Tail fin wounding Zebrafish embryos at 2–3 dpf were anesthetized using 0.016% tricaine (Sigma) and then wounded on the ventral side of the tail fin with the tip of a glass capillary needle as described.[29] Wounded embryos were fixed in 4% paraformaldehyde/PBS at various time points after the wounding and stored in PBS, containing 0.01% Tween-20 (PBST) at 4 °C, for myeloid cell detection.

Microangiography Tetramethylrhodamine dextran was injected into the sinus venosus of anesthetized zebrafish embryos as described.[44] Images were acquired within ten minutes after injection.

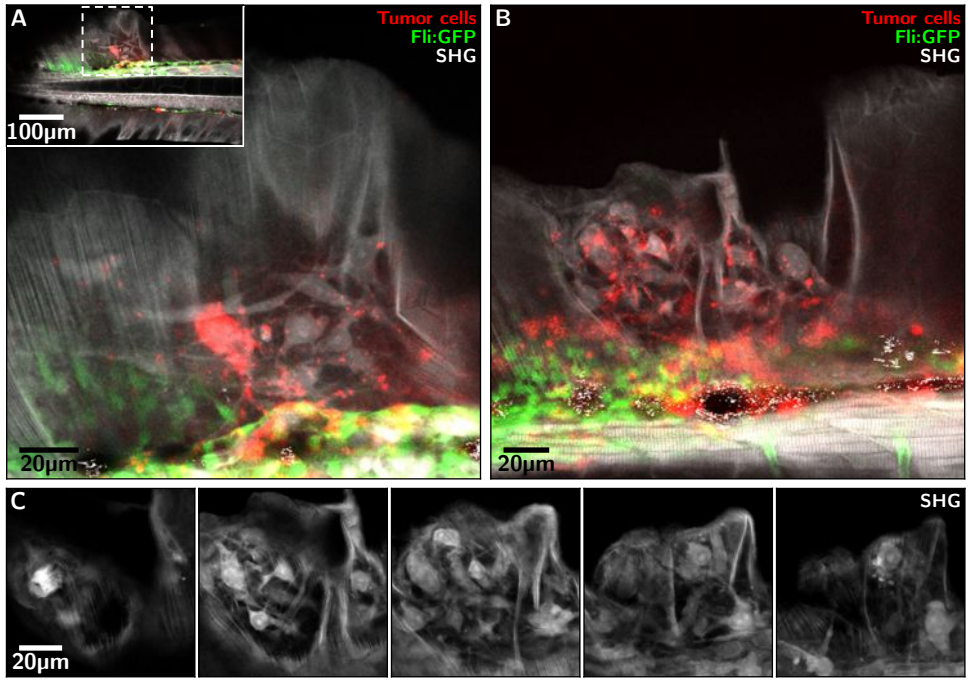

Figure 7.12:
SHG analysis of the collagen matrix around the micrometastis at 6 dpi.
(A,B) Tumor cells are labeled with the red cell tracker CM-DiL, resulting in a dotted fluorescent pattern in which proliferating cells have less signal. The vasculature is labeled green. The tumor cells seem to have pushed away the original collagen structure of the fin.
(C) Individual cross-sections from the tumor of (B), taken 7µm apart, show how the collagen structure encapsulates the tumor in all three dimensions.

Statistical analysis Statistical analysis was performed using the Prism 4 software (GraphPad), two- or one-tailed, unpaired t-tests with confidence intervals of 90% or 95%. ns = not significant ($p > 0.05$); * = $0.01 < p < 0.05$; ** = $0.0001 < p < 0.01$; *** = $p < 0.0001$.

7.6 Possibilities for new studies

The ability to non invasively image the collagen network of zebrafish, can be used to study many other processes. In this section we describe a few of the possibilities.

When tumor cells invade new tissue, the original ECM has to remodel to make space for the fast growing tumor. Figure 7.12 shows how the original collagen structure of the zebrafish fin seems to be pushed away by the new tumor tissue.

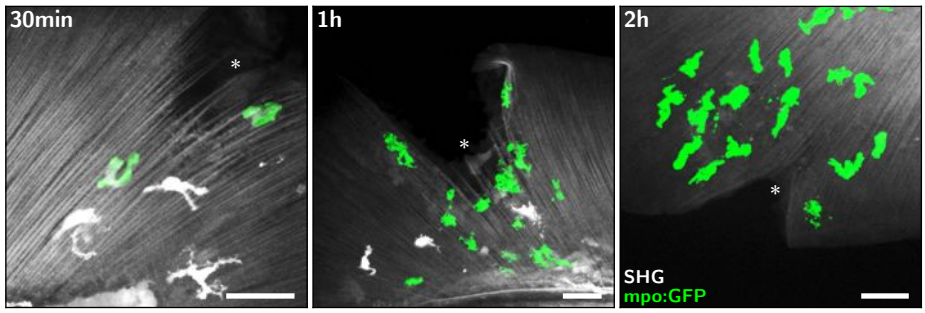

Figure 7.13:
Migrating mpo:GFP labeled neutrophils near a wound, marked by *, at 30 min, 1 h and 2 h post wounding. Already within 30 min after wounding, the first neutrophils arrive at the wounding site. Unlike the migrating neutrophils in the cancer model, fig. 7.9, these neutrophils do not seem to leave any tracks in the collagen matrix.

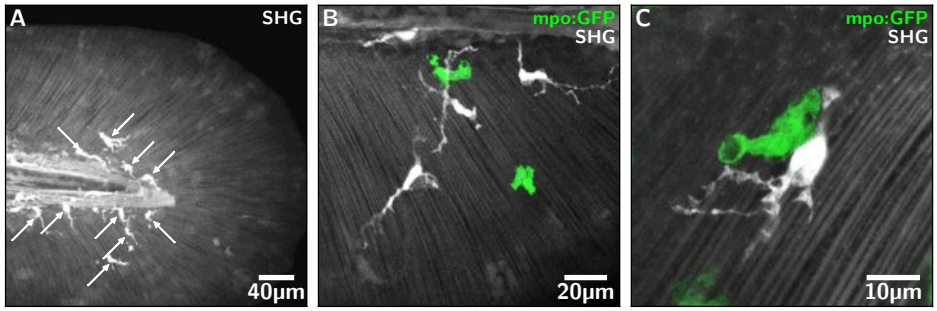

Figure 7.14:
Unknown cells, marked with arrows in (A), are visible in the second harmonic signal in the tail of zebrafish embryos. These cells seem to interact with the collagen fibers (B) and with neutrophils (C).

Figure 7.13 shows how the neutrophils indeed migrate towards the wound within 30 minutes after wounding. However, no obvious track of deformed collagen matrix was observed. It is possible that the neutrophil interact differently with collagen matrix during the pathological migration induced by wounding-induced inflammation, comparing to their physiological random migration (as shown in fig. 7.9). In addition, we noticed that the SHG signals around the wound are weaker than the non-wounded area, which makes it harder to detect deformed collagen tracks. The reduction of collagen SHG signal may be caused by the H_2O_2 production of the local tissue at the wound, which was recently discovered as the chemotractant for neutrophils to rapidly detect a wound in zebrafish.[45] We have noticed that the collagen SHG signal significantly decreased when the embryos were treated with 0.015% H_2O_2, supporting the hypothesis

that the H_2O_2 produced by wounded tissue weaken the collagen SHG signal (via an unknown mechanism).

In some of the multi-photon images, unknown cells are visible in the SHG signal, fig. 7.14. These cells seem to interact with the collagen matrix, fig. 7.14B, and possibly with neutrophils, fig. 7.14C. Immunological staining showed that these cells are neither macrophages nor fibroblasts. Further measurements are needed to understand what kind of cells these are, how they generate a second-harmonic signal and, more interestingly, what their interactions with the collagen matrix are.

7.7 Acknowledgements

We thank M. Presta and P. ten Dijke for providing cell lines; R.C. Hoeben for lenti-viral viruses; B. Weinstein and S. Renshaw for providing zebrafish lines; A. Huttenlocher for providing antibody; W. van der Ent, M.J. Rabelink and S. Rueb for assistance in cell culture and generation of stable fluorescent cell lines; A. van der Laan for support in multi-photon microscopy; D. de Witt and U. Nehrdich for zebrafish maintenance; M. Mione, P. ten Dijke and T.H. Oosterkamp for stimulating discussions; E.E. Patton for critical reading of the manuscript. This project was financially supported by the European Community under the FP7 ZF-Cancer project (HEALTH-F2-2008-201439).

7.8 References

[1] A. Patenaude, J. Parker, and A. Karsan. Involvement of endothelial progenitor cells in tumor vascularization. *Microvasc. Res.*, 79:217, 2010.

[2] J. A. Joyce and J. W. Pollard. Microenvironmental regulation of metastasis. *Nat. Rev. Cancer*, 9:239, 2009.

[3] L. M. Vecchiarelli-Federico, et al. Vascular Endothelial Growth Factor-A Positive and Negative Regulator of Tumor Growth. *Cancer Res.*, 70:863, 2010.

[4] C. Stockmann, et al. Deletion of vascular endothelial growth factor in myeloid cells accelerates tumorigenesis. *Nature*, 456:814, 2008.

[5] T. D. Tlsty and L. M. Coussens. Tumor stroma and regulation of cancer development. *Annu. Rev. Pathol.*, 1:119, 2006.

[6] M. Aghi and E. A. Chiocca. Contribution of bone marrow-derived cells to blood vessels in ischemic tissues and tumors. *Mol. Ther.*, 12:994, 2005.

[7] F. Shojaei and N. Ferrara. Refractoriness to antivascular endothelial growth factor treatment: role of myeloid cells. *Cancer Res.*, 68:5501, 2008.

[8] K. Stoletov and R. Klemke. Catch of the day: zebrafish as a human cancer model. *Oncogene*, 27:4509, 2008.

[9] G. J. Lieschke and N. S. Trede. Fish immunology. *Curr. Biol.*, 19:R678, 2009.

[10] W. Goessling, T. E. North, and L. I. Zon. New waves of discovery: modeling cancer in zebrafish. *J. Clin. Oncol.*, 25:2473, 2007.

[11] T. E. North, et al. Prostaglandin E2 regulates vertebrate haematopoietic stem cell homeostasis. *Nature*, 447:1007, 2007.

[12] L. I. Zon and R. T. Peterson. In vivo drug discovery in the zebrafish. *Nat. Rev. Drug Discov.*, 4:35, 2005.

[13] N. D. Lawson and B. M. Weinstein. In vivo imaging of embryonic vascular development using transgenic zebrafish. *Dev. Biol.*, 248:307, 2002.

[14] S. A. Renshaw, et al. A transgenic zebrafish model of neutrophilic inflammation. *Blood*, 108:3976, 2006.

[15] Y. Feng, et al. Live Imaging of Innate Immune Cell Sensing of Transformed Cells in Zebrafish Larvae: Parallels between Tumor Initiation and Wound Inflammation. *PLoS Biol.*, 8:e1000562, 2010.

[16] K. Stoletov, et al. High-resolution imaging of the dynamic tumor cell vascular interface in transparent zebrafish. *PNAS*, 104:17406, 2007.

[17] A. T. Chen and L. I. Zon. Zebrafish Blood Stem Cells. *J. Cell. Biochem.*, 108:35, 2009.

[18] F. Ellett and G. J. Lieschke. Zebrafish as a model for vertebrate hematopoiesis. *Curr. Opin. Pharmacol.*, 10:563, 2010.

[19] J. R. Mathias, et al. Live imaging of chronic inflammation caused by mutation of zebrafish Hai1. *J. Cell. Sci.*, 120:3372, 2007.

[20] M. Haldi, C. Ton, W. L. Seng, and P. McGrath. Human melanoma cells transplanted into zebrafish proliferate, migrate, produce melanin, form masses and stimulate angiogenesis in zebrafish. *Angiogenesis*, 9:139, 2006.

[21] S. Nicoli, D. Ribatti, F. Cotelli, and M. Presta. Mammalian tumor xenografts induce neovascularization in zebrafish embryos. *Cancer Res.*, 67:2927, 2007.

[22] J. Rhodes, et al. Interplay of pu.1 and gata1 determines myelo-erythroid progenitor cell fate in zebrafish. *Dev. Cell*, 8:97, 2005.

[23] F. Su, et al. Differential regulation of primitive myelopoiesis in the zebrafish by Spi-1/Pu.1 and C/ebp1. *Zebrafish*, 4:187, 2007.

[24] F. Ellett, et al. mpeg1 promoter transgenes direct macrophage-lineage expression in zebrafish. *Blood*, 117:e49, 2011.

[25] C. Gray, et al. Simultaneous intravital imaging of macrophage and neutrophil behaviour during inflammation using a novel transgenic zebrafish. *Thromb. Haemost.*, 105:811, 2011.

[26] A. Zoumi, A. Yeh, and B. J. Tromberg. Imaging cells and extracellular matrix in vivo by using second-harmonic generation and two-photon excited fluorescence. *PNAS*, 99:11014, 2002.

[27] C. Gaggioli, et al. Fibroblast-led collective invasion of carcinoma cells with differing roles for RhoGTPases in leading and following cells. *Nat. Cell Biol.*, 9:1392, 2007.

[28] L. K. Mathew, et al. Unraveling tissue regeneration pathways using chemical genetics. *J. Biol. Chem.*, 282:35202, 2007.

[29] J. R. Mathias, et al. Resolution of inflammation by retrograde chemotaxis of neutrophils in transgenic zebrafish. *J. Leukoc. Biol.*, 80:1281, 2006.

[30] K. Kissa and P. Herbomel. Blood stem cells emerge from aortic endothelium by a novel type of cell transition. *Nature*, 464:112, 2010.

[31] J. Y. Bertrand, et al. Haematopoietic stem cells derive directly from aortic endothelium during development. *Nature*, 464:108, 2010.

[32] R. M. White, et al. DHODH modulates transcriptional elongation in the neural crest and melanoma. *Nature*, 471:518, 2011.

[33] C. J. Ceol, et al. The histone methyltransferase SETDB1 is recurrently amplified in melanoma and accelerates its onset. *Nature*, 471:513, 2011.

[34] K. B. Walters, et al. Live imaging of neutrophil motility in a zebrafish model of WHIM syndrome. *Blood*, 116:2803, 2010.

[35] Q. Deng, et al. Dual roles for Rac2 in neutrophil motility and active retention in zebrafish hematopoietic tissue. *Dev. Cell*, 21:735, 2011.

[36] I. J. Fidler. The pathogenesis of cancer metastasis: the 'seed and soil' hypothesis revisited. *Nat. Rev. Cancer*, 3:453, 2003.

[37] D. Hanahan and R. A. Weinberg. Hallmarks of cancer: the next generation. *Cell*, 144:646, 2011.

[38] H. K. Jensen, et al. Presence of intratumoral neutrophils is an independent prognostic factor in localized renal cell carcinoma. *J. Clin. Oncol.*, 27:4709, 2009.

[39] M. Wislez, et al. Hepatocyte growth factor production by neutrophils infiltrating bronchioloalveolar subtype pulmonary adenocarcinoma: role in tumor progression and death. *Cancer Res.*, 63:1405, 2003.

[40] S. F. G. Krens, et al. Distinct functions for ERK1 and ERK2 in cell migration processes during zebrafish gastrulation. *Dev. Biol.*, 319:370, 2008.

[41] M. Deckers, et al. The tumor suppressor Smad4 is required for transforming growth factor beta-induced epithelial to mesenchymal transition and bone metastasis of breast cancer cells. *Cancer Res.*, 66:2202, 2006.

[42] S. He, et al. Genetic and transcriptome characterization of model zebrafish cell lines. *Zebrafish*, 3:441, 2006.

[43] S. He, et al. A ΔRaf1-ER-inducible oncogenic zebrafish liver cell model identifies hepatocellular carcinoma signatures. *J. Pathol.*, 225:19, 2011.

[44] M. Montero-Balaguer, et al. Stable Vascular Connections and Remodeling Require Full Expression of VE-Cadherin in Zebrafish Embryos. *PLoS ONE*, 4:e5772, 2009.

[45] P. Niethammer, C. Grabher, A. T. Look, and T. J. Mitchison. A tissue-scale gradient of hydrogen peroxide mediates rapid wound detection in zebrafish. *Nature*, 459:996, 2009.